J|A|C|S

JOURNAL OF THE AMERICAN CHEMICAL SOCIETY

Designing Polar and Magnetic Oxides: Zn_2FeTaO_6 - in Search of Multiferroics

Man-Rong Li,[†] Peter W. Stephens,[‡] Maria Retuerto,[†] Tapati Sarkar,[†] Christoph P. Grams,[§] Joachim Hemberger,[§] Mark C. Croft,[‖] David Walker,[⊥] and Martha Greenblatt*,[†]

[†]Department of Chemistry and Chemical Biology, Rutgers, the State University of New Jersey, 610 Taylor Road, Piscataway, New Jersey 08854, United States

[‡]Department of Physics & Astronomy, State University of New York, Stony Brook, New York 11794, United States

[§]II. Physikalisches Institut, Universität zu Köln, D 50937 Köln, Germany

[‖]Department of Physic and Astronomy, Rutgers, the State University of New Jersey, 136 Frelinghusen Road, Piscataway, New Jersey 08854, United States

[⊥]Lamont Doherty Earth Observatory, Columbia University, 61 Route 9W, PO Box 1000, Palisades, New York 10964, United States

S *Supporting Information*

ABSTRACT: Polar oxides are technically of great interest but difficult to prepare. Our recent discoveries predicted that polar oxides can be synthesized in the corundum-derivative $A_2BB'O_6$ family with unusually small cations at the A-site and a d^0 electron configuration ion at B'-site. When magnetic transition-metal ions are incorporated more interesting polar magnetic oxides can form. In this work we experimentally verified this prediction and prepared $LiNbO_3$ (LN)-type polar magnetic Zn_2FeTaO_6 via high pressure and temperature synthesis. The crystal structure analysis indicates highly distorted ZnO_6 and (Fe/Ta)O_6 octahedra, and an estimated spontaneous polarization (P_S) of $\sim$50 μC/cm^2 along the c-axis was obtained from point charge model calculations. $Zn_2Fe^{3+}Ta^{5+}O_6$ has a lower magnetic transition temperature ($T_N \sim 22$ K) than the Mn_2FeTaO_6 analogue but is less conductive. The dielectric and polarization measurements indicate a potentially switchable component.

The study of polar materials has become an important topic of materials science due to the fundamental and technological opportunities arising from their interesting and useful physical properties,[1,2] including pyroelectric, piezoelectric, ferroelectric, multiferroic behavior, and second harmonic generation (SHG) effect. When magnetic ions are incorporated into polar materials and, in the rare cases, when strong coupling between magnetization and polarization occurs, the so-called magnetoelectric effect allows magnetic control of the electrical polarization and *vice versa* for multiple-state memory applications. However, materials with both magnetic and ferroelectric polarization are difficult to prepare because of the conflicting electronic requirements of these properties,[3,4] and therefore only a few multiferroic materials are known to date. So far, perovskites (ABO_3) and related oxides are the most promising and widely studied multiferroic systems. One strategy to produce ferroelectric polarization in perovskites is to locate a lone pair electron active cation at the A-site, such as Pb^{2+} or Bi^{3+} where the stereochemical effect of the nonbonding $6s^2$ lone pair electron drives the electric polarization, as observed in $BiFeO_3$[5,6] and $PbVO_3$.[7] There are only a few elements with a lone electron pair, and the presence of such element is not a guarantee for a polar structure, e.g., $BiScO_3$[8] and $BiGaO_3$.[6] A second approach to obtain ferroelectricity is via structural distortion. Examples are the polar $LiNbO_3$ (LN)-type compounds, which contain unusually small A-site cations and may be considered as highly distorted perovskite-based structures with small tolerance factors (t) and octahedral coordination for both the A- and B-site cations, such as $ScFeO_3$,[9] $(In_{1-x}\square_x)MO_{3-\delta}$ (M = Mn/Fe, $\square$ = vacancy),[10] $FeTiO_3$,[11] and $MnMO_3$ (M = Ti, Sn).[12] In these compounds the polarization arises from the structural distortions due to atomic displacements and octahedral distortions (Section 1, Supporting Information (SI)). This strategy does not require the presence of lone pair electron cations and thus provides more opportunities in the search and design of new polar materials.

We recently expanded the LN-type structure to the $A_2BB'O_6$ system.[13] For the high pressure and temperature (HPT) synthesized $Mn_2^{2+}Fe^{3+}M^{5+}O_6$ (M = Nb, and Ta) the calculated spontaneous polarizations are 32 and 23 μC·cm^{-1} for M = Nb and Ta, respectively; magnetic ordering (T_N) is observed above 200 K, due to magnetic interactions between the high spin (HS) d^5 electrons of Mn^{2+} and Fe^{3+}. Moreover, significant pyroelectric response at low temperature and SHG effect was also observed. First-principle theoretical calculations revealed that the polarization in Mn_2FeMO_6 is due to the second-order Jahn–Teller (SOJT) effect of d^0 ions Nb^{5+} and Ta^{5+}. These findings suggested many new LN-type materials in the $A_2BB'O_6$ system, because of the large variety of ions that the structure can accommodate and the structural versatility of the cation arrangements. With these considerations we predicted possible novel polar compounds in the $A_2^{2+}B^{3+}B'^{5+}O_6$ and $A_2^{2+}B^{2+}B'^{6+}O_6$ series, where A is an unusually small cation and B' is a d^0 ion. In this paper, we present the synthesis at HPT and characterization of LN-type Zn_2FeTaO_6 and confirm the

validity of our prediction. High-resolution synchrotron powder X-ray diffraction (SPXD) analysis and dielectric and polarization studies were also performed to understand the experimental data at the microscopic level.

The small tolerance factor of Zn_2FeTaO_6 (0.836)[14] predicts unstable perovskite structure under ambient pressure, which was confirmed by experiments (Figure S2). Subsequent HPT synthesis at 1623 K under 9 GPa of pure polycrystalline Zn_2FeTaO_6 was demonstrated by powder X-ray diffraction (PXD) analysis (Figure S2; experimental details and the crystallographic information file (CIF) are provided in SI). The phase purity and rhombohedral cell dimensions (a = 5.1709(2) Å, c = 13.9353(4) Å) of the as-prepared sample were further confirmed by high-resolution SPXD, which suggested possible space groups: the centrosymmetric $R\bar{3}c$ (no. 167, corundum-type structure) or the noncentrosymmetric $R3c$ (no. 161, LN-type structure). Although these space groups have the same reflection conditions, Rietveld refinements using the SPXD data yielded poor fit of the corundum structure (R_p/R_{wp} = 7.55/10.66%, χ^2 = 2.52) and confirmed unambiguously the noncentrosymmetric LN structure (R_p/R_{wp} = 5.82/7.72%, χ^2 = 1.32, Figure 1). The final refined structural parameters are listed in Table 1.

The LN-type crystal structure of Zn_2FeTaO_6 (inset of Figure 1a) contains corner-sharing ZnO_6 and $(Fe/Ta)O_6$ octahedral sublattices interconnected via face-sharing along the c-axis and edge-sharing in the ab-plane to form face- and edge-sharing octahedral dimers with heterometal sites (Figure S1). To overcome the electrostatic repulsions, Zn and disordered Fe/Ta in the face-sharing octahedral pairs displace away from the octahedral centroids (dashed circles in Figure 1b) by 0.542(1) (d_{Zn}) and 0.111(1) Å ($d_{Fe/Ta}$), respectively, in opposite directions along the c-axis. These displacements (d_{Zn} and $d_{Fe/Ta}$) generate three short and three long metal−oxygen bonds in $(Fe/Ta)O_6$ (1.951(7) and 2.077(8) Å) and ZnO_6 (1.997(7) and 2.365(7) Å) octahedra. The octahedral distortions are reflected by the distortion parameters (Δ)[15] (Table S1). The short and long Fe/Ta−O bond lengths are comparable with a difference of 0.126 Å, giving $\Delta_{Fe/Ta}$ of 9.8 × 10^{-4}, which is comparable with that of the B-site Sn in the LN-analogue $ZnSnO_3$ (Δ_{Sn} = 5 × 10^{-4}),[16,17] but smaller than Δ_{Nb} in $LiNbO_3$ (40 × 10^{-4}).[18] In contrast, the differences between the long and short Zn−O bonds are nearly three times larger (0.368 Å) than those of Fe/Ta−O, which suggest that the ZnO_6 octahedra are more distorted. Δ_{Zn} is calculated to be 71.2 × 10^{-4}, almost three times that of Δ_{Li} (18 × 10^{-4})[18] in $LiNbO_3$ and double that of Δ_{Zn} in $ZnSnO_3$[16] and $ZnTiO_3$ (38 × 10^{-4}).[19] Accordingly, the structural distortion in Zn_2FeTaO_6 results in spontaneous polarization (P_S) of ~50 μC/cm^2 along the c-axis calculated from the point charge model ($P_S = (\sum_i q(i)\delta d(i))/V$, where $q(i)$ is the nominal charge on the ith atom, $\delta d(i)$ is the displacement along the c-axis of the ith atom from its position in the pseudocentrosymmetric structure, and V is the unit cell volume).[20] This large polarization is comparable with the P_S of $ZnSnO_3$ (~58 μC/cm^2) observed on thin film[21] and somewhat smaller than that of $LiNbO_3$ (67 μC/cm^2).[22] The X-ray absorption spectra (XAS) of Fe and Ta indicated formal cation oxidation states of $Zn^{2+}_2Fe^{3+}Ta^{5+}O_6$ (Figure S3), which is consistent with the bond valence sums calculations (Table S1).

The thermal evolution of the magnetic susceptibility (χ_{dc}) of Zn_2FeTaO_6 is shown in Figure 2a. The susceptibility keeps on increasing as the temperature is decreased but lacks any sharp
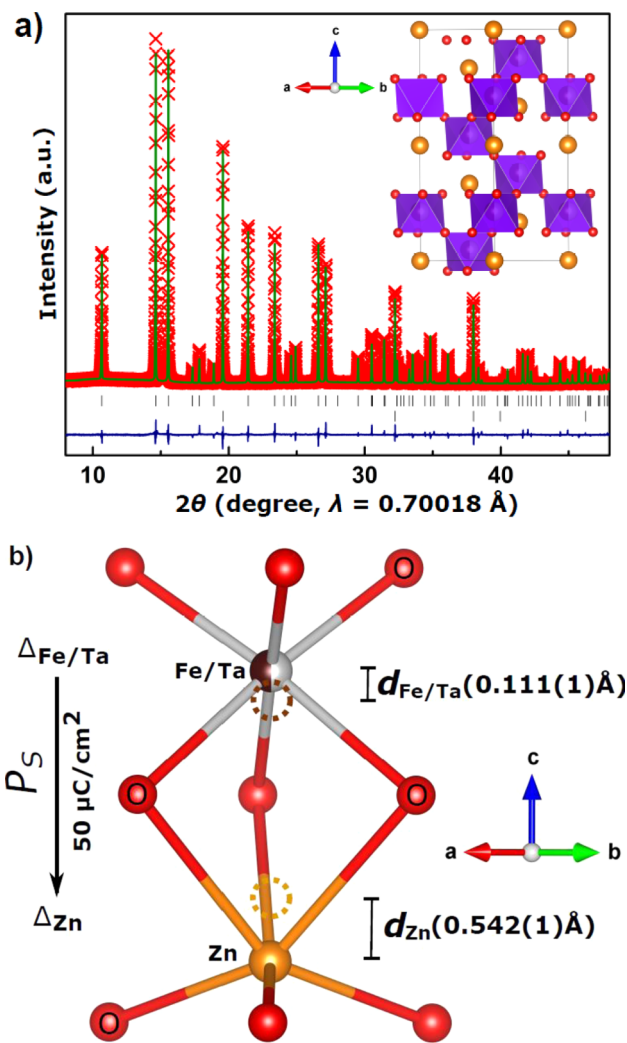

Figure 1. (a) Rietveld refinement of the SPXD data for Zn_2FeTaO_6. Red cross represents the observed data, the green line the calculated fit, the deep blue line the difference, upper and lower black tick marks the peak positions of Zn_2FeTaO_6 and diamond (internal standard), respectively. Inset shows the crystal structure viewed along [110] direction. Zn, orange spheres; $(Fe/Ta)O_6$ octahedra, purple; O, red spheres. (b) Crystal structure of the face-sharing $ZnO_6/(Fe/Ta)O_6$ octahedral pair. The atomic displacements (ds) away from the ZnO_6 and $(Fe/Ta)O_6$ octahedral site centroids (highlighted by dashed circles) are indicated as d_{Zn} (0.542(1) Å) and $d_{Fe/Ta}$ (0.111(1) Å), respectively. P_S is for the spontaneous polarization.

Table 1. Refined Structural Parameters in Zn_2FeTaO_6 from SPXD Data Collected at Room Temperature[a]

atom	site	x	y	z	B, Å^2 [b]
Zn	6a	0	0	0	0.39(1)
Fe/Ta[c]	6a	0	0	0.2135(1)	0.39(1)
O	18b	0.034(1)	0.334(2)	0.2889(6)	0.39(1)

[a]Rhombohedral, space group $R3c$ (no. 161), a = 5.1709(2) Å, c = 13.9353(4) Å, V = 322.68(3) Å^3, Z = 3, R_{wp} = 7.72%, R_p = 5.82%, χ^2 = 1.32. [b]Isotropic atomic displacement parameters (B) were constrained to be the same value. [c]Occupancy of Fe/Ta site slightly deviated from half/half and thus fixed to 0.5/0.5 during the refinements.

transition, which indicates the absence of proper long-range order. At low temperature ($T \sim$ 22 K), the zero field cooled (ZFC) curve shows a cusp-like feature (marked by the blue
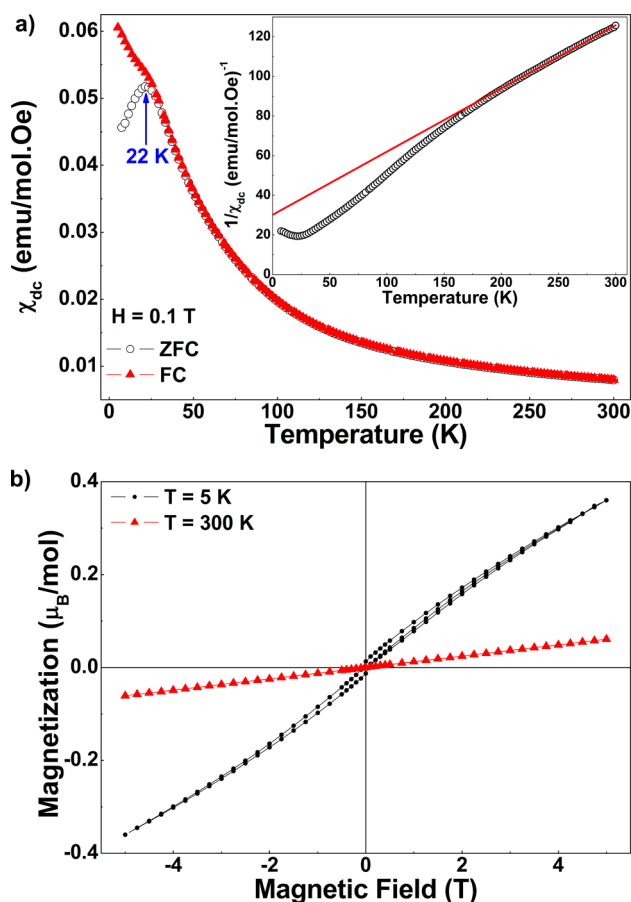
Figure 2. Magnetic behavior of Zn_2FeTaO_6. (a) Temperature dependence of the ZFC and FC dc susceptibility (χ_{dc}) at 1000 Oe, inset shows the susceptibility inverse ($1/\chi_{dc}$) vs temperature plot. (b) Isothermal magnetization measured at 5 and 300 K, respectively.

153 arrow in Figure 2a). This cusp-like feature, along with the fact
154 that the ZFC and field cooled (FC) curves diverge below 22 K,
155 is reminiscent of systems undergoing spin glass-like transitions
156 and may well suggest the presence of magnetic frustration in
157 this system, with competing short-range ferromagnetic (FM)
158 and antiferromagnetic (AFM) interactions. Although the
159 sample exhibits no clear long-range magnetic transition, the
160 inverse susceptibility data ($1/\chi_{dc}$) reveal a deviation from strict
161 linearity at temperatures below 200 K (inset of Figure 2a).
162 Hence we fit the data above 200 K to the Curie−Weiss law $\chi =$
163 $C/T - \theta_{CW}$ (red line in the inset of Figure 2a). The fitting
164 allowed us to extract the value of the effective magnetic
165 moment $\mu_{eff} = 4.99\ \mu_B$. This is slightly less than the calculated
166 spin only moment per formula unit ($\mu_{cal} = 5.92\ \mu_B$) of Fe^{3+},
167 probably due to the disordering of the Fe and Ta ions. The
168 Curie−Weiss constant ($\theta_{CW} = -94$ K) indicates the presence of
169 dominant AFM interactions. Figure 2b presents the isothermal
170 magnetization (M) vs H curves of Zn_2FeTaO_6 recorded at 5
171 and 300 K, respectively. At 300 K, the sample is in the
172 paramagnetic state, while at 5 K, it shows a small hysteresis with
173 a coercive field $H_C \sim 0.07$ T. This might be indicative of the
174 presence of some FM interactions in the system at low
175 temperature. However, even at this temperature the $M-H$
176 curve shows no sign of saturation, which indicates the presence
177 of competing AFM interactions that might lie at the root of the
178 magnetic frustration.

Compared with the isostructural Mn_2FeTaO_6,[13] the replace- 179
ment of the magnetic Mn^{2+} by the diamagnetic Zn^{2+} dilutes the 180
magnetic interactions in the system and increases the electric 181
resistance as reflected by the dielectric measurements (Figure 182 f3
3a,b). The dielectric behavior of Zn_2FeTaO_6 is similar to that of 183 f3
Mn_2FeTaO_6[13] and other analogues,[23] showing a high-ε contact 184
feature near room temperature and no sign of (switchable) 185
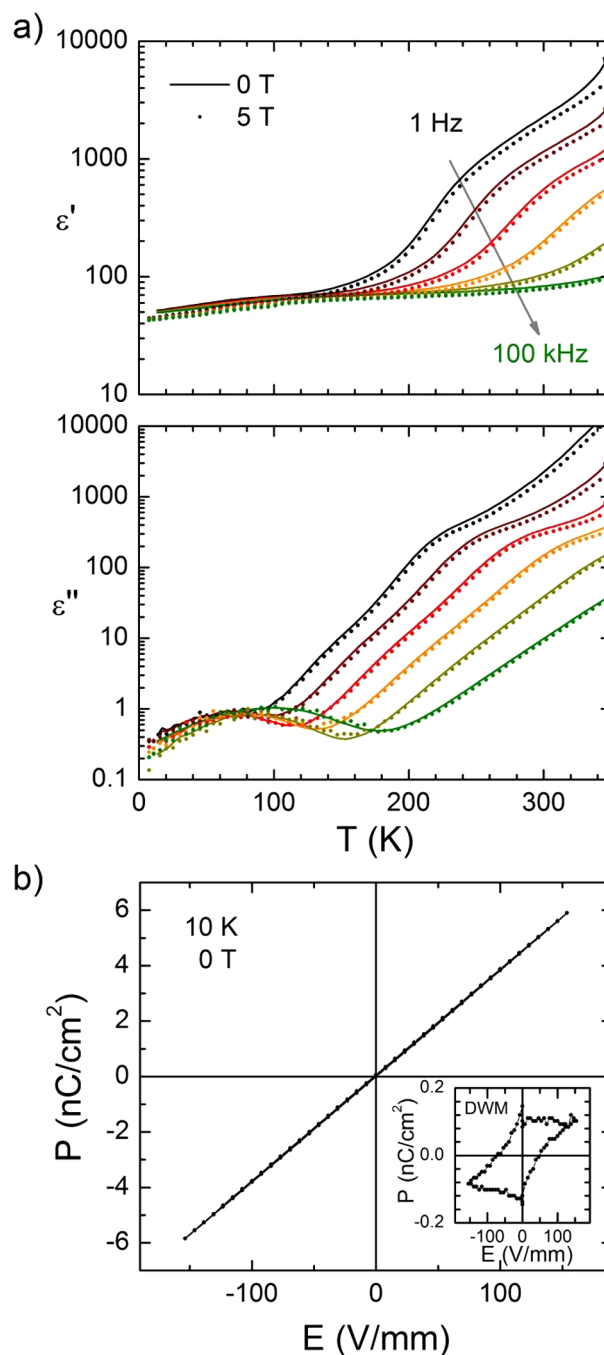
Figure 3. Dielectric properties of Zn_2FeTaO_6. (a) Temperature dependence of the dielectric function (ε) is dominated by a contact feature that masks the intrinsic value of ε for temperatures higher than 100 K. Only at low temperatures the intrinsic value $\varepsilon \approx 50$ can be measured. (b) Electric-field-dependent polarization measurements at 10 K in zero magnetic field show a nearly flat "loop" and also the result of the DWM[24] gives only very small values for the switchable polarization as shown in the inset.

ferroelectricity. The polarization-electric field ($P(E)$) "loop" at low temperature is nearly completely flat (as in paraelectrics in Figure 3b), the inset of Figure 3b denotes the difference between the first and second half-cycle of the double wave method (DWM)[24] and gives very small values, which can be understood as experimental resolution giving a lower boundary for a possible switchable component in the multidomain polycrystalline sample. The small differences in the temperature-dependent permittivity for zero field and 5 T data are probably due to a small magnetoresistive contribution altering the effective RC-element of the contacts/grain boundaries. Further exploration of ferroelectric transition in monodomain thin films or single crystal samples of Zn_2FeTaO_6 is planned similar to those of $ZnSnO_3$, where not the bulk, only the film sample showed switchable polarization.[21]

In conclusion, the successful synthesis and study of the novel polar and magnetic $LiNbO_3$-type Zn_2FeTaO_6 in this work further confirmed the theoretical prediction for polar structures in the $A^{2+}_2B^{3+}B'^{5+}O_6$ corundum-based family with a d^0 electron configuration ion at the B'-site. The designed polar structure and multifunctional properties in Zn_2FeTaO_6 suggest strong potential in search of multifunctional materials in $A_2BB'O_6$ phases, especially ferroelectric materials with Al^{3+}, Ga^{3+}, or Sc^{3+} at the B-site and multiferroic materials with transition metals at both the B- and B'-sites and Zn^{2+} or Mg^{2+} at the A-site.

■ ASSOCIATED CONTENT

ⓈSupporting Information

Comparison of the perovskite and $LiNbO_3$ type crystal structures, details of high and ambient pressure syntheses, powder synchrotron X-ray diffraction studies and crystallographic data, X-ray absorption spectroscopy analysis, magnetic, dielectric, and ferroelectric measurements. This material is available free of charge via the Internet at http://pubs.acs.org.

■ AUTHOR INFORMATION

Corresponding Author

martha@rutchem.rutgers.edu

Notes

The authors declare no competing financial interest.

■ ACKNOWLEDGMENTS

■ REFERENCES

(1) Ok, K. M.; Chi, E. O.; Halasyamani, P. S. *Chem. Soc. Rev.* **2006**, *35*, 710.

(2) Rao, C. N. R.; Sundaresan, A.; Saha, R. *J. Phys. Chem. Lett.* **2012**, *3*, 2237.

(3) Hill, N. A. *J. Phys. Chem. B* **2000**, *104*, 6694.

(4) Donakowski, M. D.; Gautier, R.; Yeon, J.; Moore, D. T.; Nino, J. C.; Halasyamani, P. S.; Poeppelmeier, K. R. *J. Am. Chem. Soc.* **2012**, *134*, 7679.

(5) Wang, J.; Neaton, J. B.; Zheng, H.; Nagarajan, V.; Ogale, S. B.; Liu, B.; Viehland, D.; Vaithyanathan, V.; Schlom, D. G.; Waghmare, U. V.; Spaldin, N. A.; Rabe, K. M.; Wuttig, M.; Ramesh, R. *Science* **2003**, *299*, 1719.

(6) Belik, A. A. *J. Solid State Chem.* **2012**, *195*, 32.

(7) Singh, D. J. *Phys. Rev. B* **2006**, *73*, 094102.

(8) Belik, A. A.; Iikubo, S.; Kodama, K.; Igawa, N.; Shamoto, S.-i.; Maie, M.; Nagai, T.; Matsui, Y.; Stefanovich, S. Y.; Lazoryak, B. I.; Takayama-Muromachi, E. *J. Am. Chem. Soc.* **2006**, *128*, 706.

(9) Li, M.-R.; Adem, U.; McMitchell, S. R. C.; Xu, Z.; Thomas, C. I.; Warren, J. E.; Giap, D. V.; Niu, H.; Wan, X.; Palgrave, R. G.; Schiffmann, F.; Cora, F.; Slater, B.; Burnett, T. L.; Cain, M. G.; Abakumov, A. M.; van Tendeloo, G.; Thomas, M. F.; Rosseinsky, M. J.; Claridge, J. B. *J. Am. Chem. Soc.* **2012**, *134*, 3737.

(10) Belik, A.; Furubayashi, T.; Matsushita, Y.; Tanaka, M.; Hishita, S.; Takayama-Muromachi, E. *Angew. Chem., Int. Ed.* **2009**, *48*, 6117.

(11) Varga, T.; Kumar, A.; Vlahos, E.; Denev, S.; Park, M.; Hong, S.; Sanehira, T.; Wang, Y.; Fennie, C. J.; Streiffer, S. K.; Ke, X.; Schiffer, P.; Gopalan, V.; Mitchell, J. F. *Phys. Rev. Lett.* **2009**, *103*, 047601.

(12) Aimi, A.; Katsumata, T.; Mori, D.; Fu, D.; Itoh, M.; Kyômen, T.; Hiraki, K.-i.; Takahashi, T.; Inaguma, Y. *Inorg. Chem.* **2011**, *50*, 6392.

(13) Li, M.-R.; Walker, D.; Retuerto, M.; Sarkar, T.; Hadermann, J.; Stephens, P. W.; Croft, M.; Ignatov, A.; Grams, C. P.; Hemberger, J.; Nowik, I.; Halasyamani, P. S.; Tran, T. T.; Mukherjee, S.; Dasgupta, T. S.; Greenblatt, M. *Angew. Chem., Int. Ed.* **2013**, *52*, 8406.

(14) Lufaso, M. W.; Woodward, P. M. *Acta Crystallogr., Sect. B* **2001**, *57*, 725.

(15) Brown, I. D.; Shannon, R. D. *Acta Crystallogr., Sect. A* **1973**, *29*, 266.

(16) Inaguma, Y.; Yoshida, M.; Katsumata, T. *J. Am. Chem. Soc.* **2008**, *130*, 6704.

(17) Hoel, C. A.; Amores, J. M. G.; Morán, E.; Álario-Franco, M. A.; Gaillard, J.-F.; Poeppelmeier, K. R. *J. Am. Chem. Soc.* **2010**, *132*, 16479.

(18) Hsu, R.; Maslen, E. N.; Boulay, D. d.; Ishizawa, N. . *Acta Crystallogr., Sect. B* **1997**, *53*, 420.

(19) Inaguma, Y.; Aimi, A.; Shirako, Y.; Sakurai, D.; Mori, D.; Kojitani, H.; Akaogi, M.; Nakayama, M. *J. Am. Chem. Soc.* **2014**, *136*, 2748.

(20) Resta, R.; Vanderbilt, D. *Theory of Polarization: A Modern Approach*; Springer: Berlin, Heidelberg, 2007, *105*, 31.

(21) Son, J. Y.; Lee, G.; Jo, M.-H.; Kim, H.; Jang, H. M.; Shin, Y.-H. *J. Am. Chem. Soc.* **2009**, *131*, 8386.

(22) Hsu, R.; Maslen, E. N.; du Boulay, D.; Ishizawa, N. *Acta Crystallogr., Sect. B* **1997**, *53*, 420.

(23) Inaguma, Y.; Sakurai, D.; Aimi, A.; Yoshida, M.; Katsumata, T.; Mori, D.; Yeon, J.; Halasyamani, P. S. *J. Solid State Chem.* **2012**, *195*, 115.

(24) Fukunaga, M.; Noda, Y. *J. Phys. Soc. Jpn.* **2008**, *77*, 064706.